A Battery-Powered Soft Electromechanical Stimulation Patch for Haptic Human-Machine Interfaces

Junwen Zhong (junwenzhong@um.edu.mo)
University of Macau
Wenying Qiu
University of California at Berkeley
Tao Jiang
Tsinghua University
Archie Yao
Carnegie Mellon University https://orcid.org/0000-0001-6369-129X
Zhichun Shao
University of California at Berkeley
Qilong Cheng
University of California at Berkeley https://orcid.org/0000-0002-1281-2204
Jiaming Liang
Tsinghua University
Dongkai Wang
Tsinghua University
David Bogy
University of California, Berkeley
Min Zhang
Tsinghua University https://orcid.org/0000-0003-2219-8030
Xiaohao Wang
Tsinghua University
Liwei Lin
Berkeley Sensor and Actuator Center

Article

Keywords: Human-machine interface, Wearable electronics, Electromechanical stimulation, Soft actuator, Haptic feedback.

Posted Date: January 13th, 2021

DOI: https://doi.org/10.21203/rs.3.rs-124644/v1

Abstract

One grand challenge in haptic human-machine interface devices is to electromechanically stimulate sensations on human skins wirelessly by thin and soft patches under a low driving voltage. Here, we propose a soft haptics-feedback system using highly charged, polymeric electret films with the annulus-shape bump contact structure to induce mechanical sensations on volunteers under an applied voltage as low as 5 volts. Together with bendable lithium ion batteries and a flexible circuit board, an untethered stimulation patch is constructed for active operations of at least 2 hours with low power consumptions. As an application example, a “silent haptic communication” system is demonstrated to transmit English alphabet letters *via* the mechanical beating patterns from a patch onto the fingertip of a receiving volunteer. The analytical model, design principle, and performance characterizations can be applicable for the integrations with other devices in wearable electronics toward various applications, including AR (augmented reality) and VR (virtual reality).

Introduction

Wearable electronics having a variety of functions are desirable devices in seamless human-machine interface applications for the modern era[1–3]. These may include flexible sensors to detect environmental signs and wearable actuators to generate mechanical sensations.[5–8] Today, numerous wearable sensors have been developed in order to monitor physiological parameters relevant to human health conditions, such as electro-cardio signals, pulse waves, blood pressure, and body motions.[9–12] On the other hand, the progress of thin and wearable soft actuators attachable to human skins using the low applied voltage or even the battery power remains very challenging.[5,6,13] For example, traditional actuator systems have utilized bulky and non-wearable rigid linear resonators, eccentric rotating masses, and voice coils to generate mechanical stimulations.[14] Thin and soft actuators based on piezoelectric polymers such as polyvinylidene fluoride (PVDF) and its co-polymers have the advantages in making flexible, thin, and light-weight patches[6,15–17]. However, the high driving voltage requirements in the range of hundreds of volts are not desirable and harmful to the human body. Actuators based on dielectric elastomer polymers demand even higher driving voltages in thousands of volts due to the difficulty in producing strong electromechanical responses by thin polymer films.[18–22] In recent years, electret-based polymeric transducers have exhibited high electromechanical conversion efficiencies for applications in energy harvesters or sensors,[23–26] which could be applicable in building thin and wearable actuators for haptic human-machine interfaces.

In general, human skins have four types of tactile receptors for haptic sensations as shown in **Fig. S1A**: (1) the tactile corpuscle (Meissner’s corpuscle, MC) sensitive to the light touching and texture changes of small skin areas under low frequency actuations; (2) the lamellar corpuscle (Pacinian corpuscle, PC) sensitive to energy stimulations of large skin areas under slightly higher frequencies of mechanical actuations, (3) the bulbous corpuscle (Ruffini ending, SA-I) sensitive to mechanical tensions deep in the skin; and (4) the Merkel nerve ending corpuscle (Merkel disc, SA-II) sensitive to sustained pressures.[27,28]

The required stresses for both sustained pressure and deep in the skin are high and difficult to generate by thin and soft polymer films. As such, this work focus on the generation of low-magnitude stimulations on the MC and PC receptors based on flexible polymer films using a low driving voltage below 400 Hz. The induced shallow electromechanical vibrations are expected to induce mechanical stimulations on human skins for haptic human-machine interface applications.

A thin and wearable haptic electromechanical patch is proposed based on the “air-bubble” electret structure to accumulate and store electrostatic charges, and the annulus-shape contact design to induce high mechanical sensations. Together with a flexible lithium-ion polymer battery as the power source and a bendable control circuit board, the system can produce mechanical sensations wirelessly under a low driving voltage for human-machine interface applications up to 2 hours in the prototype, as illustrated in Fig. 1A. The “air-bubble” electret structure helps accumulating and storing electrostatic charges to result in a high internal surface potential, which reduces the driving voltage requirement. The annulus-shape contact design helps stimulating the MC and PC tactile receptors in human skins, which further reduces the threshold driving voltage for high sensation feelings. As a result, several advancements have been achieved when compared with the state-of-art works in polymer-based wearable actuators: (**i**) detectable haptic sensations on fingertips of volunteers under an ultra-low driving voltage of only 5 Volts at 300 Hz and capable of generating high output force of 147 mN with a high driving voltage of 150 Volts, which is in the same output force level as those of modern cellphones under vibration modes; (**ii**) continuous and stable haptic operations with output variations of less than 5% after 78 million actuation cycles, and the integration with a flexible battery system (7.4 Volts) and a circuit board toward practical wearable applications; and (**iii**) an application demonstration of “silent haptic communication” by transmitting English alphabet letters from the brain waves of volunteer #A via different mechanical beating patterns to the fingertip of a receiving volunteer #B.

Results And Discussion

Design strategy

The annulus-shape contact design aims to induce strong responses from both the MC and PC receptors as shown in Fig. 1B **and Fig. S1B**. The prototype bump structure has a height of 0.5-1 mm to generate the “double gradient stimulation effect” from both inner and outer surfaces[29] by inducing a large deformation and displacement on the skin to excite the MC receptors. On the other hand, the annulus-shape structure can induce the skin indentation effect[30] to transmit large energy to the PC receptors. Figure 1C illustrates different layers of the soft actuator patch based on the 12.5 μm-thick Fluorinated Ethylene Propylene (FEP, DuPont Teflon®) films as the electret materials. The “air-bubbles” design in between the two FEP layers can increase the storages of electrostatic charges for high electromechanical outputs. The detailed fabrication process and processing steps are shown in **Fig. S2**. In short, the soft actuator is composed of two FEP/Air/FEP/Al films on top and bottom locations sandwiching a wavy-shape Al/paper/Al spring structure at the middle. Each FEP/Air/FEP/Al film can store electrostatic charges induced by a Corona charging process with the negative surface potential on the exposed FEP

film side. Two FEP/Air/FEP/Al films and one Al/paper/Al layer are assembled and fixed at the boundary by a double-sided tape (3M Company). Two 165 μm-thick Polymide (PI, Bertech Company) films are adhered on the top and bottom Al electrodes as both the mechanically-supporting and electrically-isolating layer. The top PI layer is shaped into the designed surface profiles such as the annulus-shape contact structure by using a mold insert and a pressing process, as shown in **Fig. S3**.[31] When the soft actuator is pressed by the fingertip of a volunteer on the top PI structure, a simplified model including the preload is depicted in Fig. 1D and the detail working mechanism is described in the **supporting explanation 1**. When a positive electrical voltage is applied at the middle spring electrode, the system contracts due to the electrostatic force. If the applied voltage reduces to zero, the actuator recovers back to its original shape with the assistance of the spring force.[22] The trapped air bubbles in the FEP/Air/FEP electret film can capture extra electrostatic charges on their inner surfaces[32] as shown in **Fig. S4** to result in a high surface potential with increased electromechanical coupling efficiency and reduced charge leakages for improved long-term stability. The large amount of electrostatic charges can induce a high built-in electrical field (E_{in}) while the externally applied AC driving voltage can induce the external electrical field (E_{ext}). The combination of the two electrical fields results in varying electromechanical deformations controlled by the externally applied voltage. The wavy-shape Al/paper/Al spring structure functions as both the elastic mechanical spring and the common electrical electrode.

Volunteer experiments are conducted by placing a reference soft actuator and a testing actuator (the same size of 2 × 2 cm^2) side-by-side for the left and right hands of a volunteer using their index fingertips, as indicated in **Fig. S5** for a total of 20 volunteers. At the beginning of these tests, volunteers have been asked to adjust the pressure they may apply on the actuator individually to have the best haptic sensations. The measured average preload value for the 20 volunteers is around 0.8 ± 0.2 N when the applied peak-to-peak AC voltages are 10 and 20 volts, as shown in **Fig. S6**. The high applied voltage of 20 volts results in high sensation levels in all frequencies as expected and the best haptic sensation is recorded at the frequency of 300 Hz. As such, the reference actuator is driven constantly under an alternating voltage of 20 Volts at 300 Hz to give a strong haptic sensation intensity. The testing actuator is then excited under a randomly chosen applied voltage (5, 10, or 20 Volts) and frequency (10, 50, 100, 120, 140, 170, 200, 250, 300, 350, 400, or 500 Hz) for three times of each test. The haptic sensation level is labelled as “Level 0” (no sensation), “Level 1” (weak sensation), “Level 2” (similar sensation), and “Level 3” (strong sensation) as compared with that of the reference actuator and the results are plotted in Fig. 1E. As expected, a high driving voltage induces a high electromechanical deformation and results in a strong average sensation intensity. The strongest haptic sensation results are at around 300 Hz in all cases, which also agrees well with previous reports for the human skin.[27,28] The threshold or lowest AC driving voltage is at 5 Volts at 300 Hz to induce the haptic feedback sensations. For other frequencies from 50 to 400 Hz, as shown in **Fig. S7**, the required driving voltages increase slightly but they are all below 25 Volts, which is a drastically improved low value as compared with other works and it can easily meet the voltage regulation of 50 volts for human skin without the fear of the electrical shock.[33] On the other hand, the average sensation intensity in the low frequency range of 10–150 Hz increases for the actuators with the annulus-shape bump structure. This is attributed to the larger displacements generated

on the skin by the annulus-shape bump structure as compared to those of the actuators with the cylinder-shape bump or flat surface. This result is further validated by the “adapting stimulus” experiments [34–36] in **Fig. S8**. The adapting stimulus tests are conducted by stimulating the index fingertip with an actuation intensity of 9 dB above the “basic line” condition for a period of 6 min at 30 Hz and 250 Hz, respectively, to allow the textile receptors to familiarize the sensational feelings and reduce their sensing sensitivities. Afterwards, the threshold voltages to induce the haptic sensation from 30 to 400 Hz are characterized again. After the 30 Hz adaption stimulation, it is found the threshold sensation voltage clearly increases for stimulations with frequencies below 150 Hz, suggesting MC receptors are more responsive to low frequency stimulations. On the other hand, after the 250 Hz adaption stimulation, the voltage threshold sensation voltage increases almost uniformly for all frequencies, implying that both PC and MC receptors have similar responses for high frequency stimulations. The low driving voltage characteristics is in favor of various human machine interface applications under the safety regulation as well as the electrical power and circuit requirements. Figure 1F compares the state-of-art soft and thin actuators and it shows the soft actuator patches presented in this work require the lowest driving voltages of at least one or two order of lower magnitude as compared with those of other systems (details in **Table S1**),[5,37–51] which is a very desirable feature for potential practical applications.

The Electret Structure And Prototype

Figure 2A shows the optical image of a fabricated FEP/Air/FEP/Al electret film, with the enlarged view showing the detailed structure in Fig. 2B. An Al-tape is first adhered to a FEP film and the system is pressed under a wavy-shape mold insert to duplicate the wavy pattern of ~ 1 mm in width and ~ 0.2–0.5 mm in height. A second flat, 12.5 μm-thick FEP film is placed on top at the FEP side of the FEP/Al film to form air bubbles. During a -20 kV Corona charging process for 20 minutes, the two FEP films are adhered strongly due to the electrostatic field while the FEP/Air/FEP/Al film is charged with a high surface potential. The wavy-shape and high stiffness of the Al tape (**Fig. S9**) prevent the collapse of the air bubbles during the normal actuator operations in Fig. 2C to help the storage of electrostatic charges to maintain high and stable surface potentials (Fig. 2D**)**. The surface charge potential of a prototype FEP/Air/FEP/Al film in the laboratory environment has been measured for 7 days to show a typical decay and stabilization process in Fig. 2E from − 1100 to -750 Volts. If a conductive Al film is applied on the metal side of the prototype FEP/Air/FEP/Al film, the surface charges can reduce quickly to -550 Volts but it remains stable afterwards as the internal charges around the air bubbles are mostly retained. In this work, the Corona charging process is set to produce more negative charges on the FEP film since it has better capacity to capture and store negative charges.[52,53]

The displacement and output energy characterizations use the setup shown in **Fig. S10**. A 4 mm-thick PDMS film is used to emulate the tissues of the fingertip and a stiff glass piece is placed between the soft actuator and the PDMS. A preload force ($F_{Preload}$) is adjusted *via* a spring and the vibration displacement (Y_s) of the glass piece is recorded by a Laser Doppler Vibrometer (LDV). The output energy (ΔW_{peak}) is estimated as (**Supporting explanation 2**):

$$\triangle W_{peak} = 2F_{preload} Y_{S-max} \quad (1)$$

where Y_{s-max} is the maximum vibration displacement relative to the neutral position. Figure 2F shows measured output energy versus the surface potential of the FEP/Air/FEP electret film under a driving voltage of 20 Volts at 300 Hz, and a preload of 0.7 N. The surface potential of the film can be adjusted by the corona charging process (**Fig. S11**). As expected, both simulation and measurement results show linear relationship between the output energy and the surface potential at the maximum around 1.3 μJ when the surface potential is around − 450 Volts for the prototype in Fig. 2F and **Supporting explanations 1 and 3**.

Three different prototype films (size of 2 × 2 cm^2) have been tested: (1) a single-layer FEP electret film (thickness of 12.5 μm), (2) a FEP/Air/FEP/Al film (one-layer air bubbles), and (3) a FEP/Air/FEP/Air/FEP/Al electret film (two-layers air bubbles) as shown in Fig. 2G. The film with one-layer air bubbles has the best stability as it maintains about 90% of the initial output energy value after in operations for 20 hours under a driving voltage of 20 Volts at 300 Hz with a preload of 0.7 N. The initial output energy value for all tests is based on the film with one-layer air bubbles and the small degradation is the result of leaked surface charges. The stability of the film with two-layers air bubbles is not as good as the film with one-layer air bubbles because the air bubbles trapped on the top layers may collapse under the preload to result in charge neutralizations (Lower **Fig. S12**). The FEP-only film has the worst stability results as most of the electrostatic charges are on the surface and they could have leaked from external contacts during the haptic sensation tests (Upper **Fig. S12**).

Effects Of Mechanical Property

When the volunteer puts his/her fingertip on the actuator patch, a preload is applied as shown in Fig. 3A and a simplified model is developed in Fig. 3B with detailed explanation in **Supporting explanation 4**.[54] In general, the stiffness of the spring structure, the design of the contactor structure, and the preload are key parameters affecting the performances. The measured output energy with respect to the stiffness of the spring structure, under a preload of 0.7 N and a driving voltage of 20 Volts at 300 Hz is shown in Fig. 3C. For a spring structure with a stiffness of 1800 N/m under a preload of 0.7 N, a maximal output energy of 1.35 μJ is recorded. For soft actuators with the spring stiffness lower than 1800 N/m, the reduced stiffness results in a more compressed spring structure by the preload, which reduces the output energy as possible electromechanical deformations are suppressed by the preload. On the other hand, for structures with the spring stiffness higher than 1800 N/m, the high stiffness also constrains the electromechanical deformations to result in reduced output energy. As such, it is expected that a specific spring stiffness will have a matching optimal preload value for the largest output energy. The applied actuation frequency also affects the sensational feelings as shown in the measured output energy of the soft actuator with respect to the driving frequency under different preload levels with a fixed spring structure of 1800 N/m in Fig. 3D. It is found that the optimal operation condition is when a preload is 0.7 N under a frequency of 300 Hz to achieve a maximal output energy.

The shape of contactor of the soft actuator is also important to generate sensational feelings. Here, a total of 15 volunteers have been tested for prototype soft actuators with flat surface, cone-shape, cylinder-shape with the total contact areas of 2.4, 5.5, 9, and 12 mm^2, and annulus-shape (fixed bump width of 0.5 mm) bumps with the total contact areas of 2.4, 5.5, 9, and 12 mm^2, as indicated in Figs. 3E and 3F. In general, actuators with the flat surface or cone-shape bump require higher voltages and frequencies to induce sensational feelings as compared to those of cylinder-shape and annulus-shape bump structures. Actuators with the annulus-shape bump require the lowest applied voltages and frequencies than those of actuators with cylinder-shape bumps under the same contact areas. Under a fixed driving frequency of 300 Hz, an annulus-shape actuator with a contact area of 5.5 mm^2 achieves the lowest average driving voltage of 4.4 Volt for the haptic sensation. Under a fixed driving voltage of 20 Volt, this annulus-shape actuator can produce sensational feeling for a frequency as low as 13 Hz. These results suggest that the annulus-shape design with an appropriate contact area can produce the best results.

Systematic Outputs Characterization

As expected, as the driving voltage increases, the output energy and displacement of a prototype soft actuator (2 × 2 cm^2, preload of 0.7 N, spring stiffness of 1800 N/m, with driving frequencies of 50 and 300 Hz) both increase as shown in Fig. 4A. In this case, the output energy/displacement increase from 0.18 μJ/0.11 μm to 3.24 μJ/1.25 μm as the applied voltage increases from 5 to 50 Volts, respectively. The typical power consumption of the prototype actuator is recorded in Fig. 4B to be 9.97 mW under a high voltage of 150 Volts at 300 Hz. This value is at least one order of magnitude lower than those of other haptic devices with similar output ability, such as the Piezo motor (98 mW, SEMCO PHAT423535XX), the eccentric rotating mass (250 mW, Sanyo NRS2574I), and the linear resonant actuator (200 mW, AAC 1036C) in **Table S2**.[55] In practical applications to generate the haptic sensation by an applied voltage of 10 Volts, the power consumption is only 45 μW. Furthermore, the long-term stability of the actuator patch is tested for 3 days under a driving voltage of 50 Volts at 300 Hz, and a preload of 0.7 N. The one-minute output energy *vs.* time data for every 12 hours have been recorded for a total of 78 million cycles as shown in Fig. 4C. It is found that the output energy remains stable with small variations of less than 5% in this long-term stability test.

The output force of soft actuators is measured with a testing setup in **Fig. S13**, in which the output force under a given preload is recorded by a force gauge. The output forces of prototype actuators with different sizes are compared with the output forces of a smart watch and 2 cellphones (iWatch, iPhone 11, and Xiaomi 8) under the vibration modes with the setup in **Fig. S14**. All prototype actuators are driven with a voltage of 150 Volts at their own resonant frequencies (150, 140, and 120 Hz for sizes of 1 × 1, 2 × 2, and 4 × 4 cm^2) under optimal preloads of 0.5, 1, and 2 N for maximal outputs. As shown in Fig. 4D, under the 150 Volts driving voltage, prototype actuators with size of 1 × 1, 2 × 2, and 4 × 4 cm^2 have output force of 22, 74, and 147 mN, respectively, while the output force for iWatch, iPhone 11, and Xiaomi 8 under their own vibration modes are 116, 110, and 165 mN, respectively.

A Wearable Silent Haptic Communication System

Visual and acoustic devices have been widely utilized to provide feedback information, while haptic-based communications belong to the category of “silent or secretive method” as depicted in Fig. 5A. In this work, a wearable silent haptic communication system is setup as shown in Fig. 5B (detailed process flow in **Fig. S15**), where a sender is wearing an EEG headset to compose the secret code by adjusting the concentration levels of various EEG intensity signals. The signals are processed and transmitted to the actuator on the finger of the receivers and turned into corresponding mechanical beats. In this work, the soft actuator is redesigned and assembled in the form of a fingerstall (inset in Fig. 5B) *via* an origami process (details in **Fig. S16**) and the detailed operation interface is depicted in **Fig. S17**.

In a demonstration example, a random message of “BCU” is used as the designated secret code and the sender can adjust the intensity level for the EEG headset to record and send the output intensity signals with 20-second as one cycle. Figure 5C shows the EEG output intensity signal *vs.* time for 6 cycles and the average EEG output intensity value is calculated. For an average value of larger than 50, the system records the information as “1” or a “0” is recorded. The output values of “11”, “01”, and “00” are defined as “B”, “C”, and “U”, respectively, as shown in Fig. 5D. For the soft actuator, information of “1” and “0” are represented by a long 10-second (L) and a short 3-second (S) vibrational stimulation, respectively, as shown in Fig. 5E. The whole silent haptic communication process for transmitting “BCU” is shown in **Supporting Video 1**. Another successful transmission of “CUB” is demonstrated in **Fig. S18** and **Supporting Video 2**. The continuous transmission of “UCB-BUC”, which is much more difficult, is demonstrated and shown in **Supporting Video 3**. It should be noted that for well-trained volunteers as sender and receiver, the successful rate for the operation of this silent haptic communication is better than 90%.

Untethered Operations

The low driving voltage requirement and low power consumption make possible the untethered and long-term operation of the soft actuator patch with the integration of flexible battery and circuit board. By adding two flexible lithium batteries (Powersteam, PGEB0054018, 10 mAH) connected in series, the total applied voltage can reach 7.4 Volts as shown in Fig. 6A. This DC voltage is converted into AC form with a frequency range between 50–300 Hz by a DC-AC convertor (MEIBAI KDX3) on a flexible substrate as shown in Fig. 6B. The added power and driver components will not hamper the flexibility, as indicated in Fig. 6C. Under the driving voltage of 7.4 Volts and frequency of 300 Hz, the output energy values of the wired and portable prototypes are very close (**Fig. S19**). Since the total power consumption for the portable device is only about 37.8 mW, this prototype untethered system can operate for at least 2 hours.

Conclusion

Thin and soft actuator patches have been constructed to generate haptic electromechanical stimulations by utilizing the high and stable surface potential of the “air-bubble” polymeric electret film structure together with the appropriate annulus bump contactor design. These flexible patches require only less

than 5 volts to operate which is at least one order of magnitude lower than those of the state-of-art actuation systems. The integration with bendable battery and circuit board for untethered operations further advances the technology toward practical applications. As a demonstration example, a silent haptic communication system is shown as one human-machine interaction application, which can be potentially extended to other areas, such as AR, VR, and security communication, … *etc*.

Characterization. The surface potential of the samples is characterized by a Trek model 347 electrostatic voltmeter. For driving voltages of more than 10 V, a PI E-463 HVPZT amplifier is utilized and an Agilent 33220A functional generator is used to adjust the frequency. For driving voltages of less than 10 V, an Agilent 33220A functional generator is utilized. The output displacement of the actuator is measured by a Laser Doppler Vibrometer (LDV, Polytech OFV5000) and the output force of the actuator is measured by an ATI Nano 43 Force Sensor. The power consumption of a soft actuator is measured by a Keithley 6514 voltage meter, a SR570 current amplifier and a NI USB-6341 DAQ. The EEG output intensity is collected by a NeuroSky mind-wave mobile-2 EEG headset and the outputs of the EEG headset are recorded by a Bluetooth serial port and processed by the LabView software.

References

1. Nathan A, *et al.* Flexible electronics: the next ubiquitous platform. *IEEE* **100**, 1486-1517 (2012).
2. Stoppa, M. *et al*. Wearable electronics and smart textiles: a critical review. *Sensors***14,** 11957–11992 (2014).
3. Rogers J. A. Nanomesh on-skin electronics. *Nanotech.* **12**, 839-840 (2017).
4. Yu X, *et al*. Skin-integrated wireless haptic interfaces for virtual and augmented reality. *Nature* **575**, 473-479 (2019).
5. Zhong J, *et al*. A flexible piezoelectret actuator/sensor patch for mechanical Human-machine interfaces. *ACS Nano* **13**, 7107-7116 (2019).
6. Han M, et al. Three-dimensional piezoelectric polymer microsystems for vibrational energy harvesting, robotic interfaces and biomedical implants. *Electron.* **2**, 26-35 (2019).
7. Persano L, *et al*. High performance piezoelectric devices based on aligned arrays of nanofibers of poly(vinylidenefluoride-co-trifluoroethylene). *Commun.* **4**, 1633 (2013).
8. Chu Y, *et al*. Human pulse diagnosis for medical assessments using a wearable piezoelectret sensing system. *Funct. Mater*. **28**, 1803413 (2018).
9. Guo H, et al. A highly sensitive, self-powered triboelectric auditory sensor for social robotics and hearing aids. *Robot.* **3**, eaat2516 (2018).
10. Pu X, *et al*. Eye motion triggered self-powered mechnosensational communication system using triboelectric nanogenerator. *Adv.* **3**, e1700694 (2017).
11. Zang Y, *et al*. Flexible suspended gate organic thin-film transistors for ultra-sensitive pressure detection. *Commun.* **6**, 6269 (2015).

12. Zhu M, *et al.* Haptic-feedback smart glove as a creative human-machine interface (HMI) for virtual/augmented reality applications. *Adv.* **6**, eaaz8693 (2020).
13. Pacchierotti C, *et al*. Wearable haptic systems for the fingertip and the hand: taxonomy, review, and perspectives. *IEEE T. Haptics* **10**, 580-600 (2017).
14. Zhang Q. M, *et al*. An all-organic composite actuator material with a high dielectric constant. *Nature* **419**, 284-287 (2002).
15. Zhang Q. M, *et al*. Giant Electrostriction and relaxor ferroelectric behavior in electron-irradiated poly(vinylidene fluoride-trifluoroethylene) copolymer. *Science* **280**, 2101-2104 (1998).
16. Jeon J-H, *et al*. Novel biomimetic actuator based on SPEEK and PVDF. *Actuat. B-Chem.* **143**, 357-364 (2009).
17. Li C-H, *et al*. A highly stretchable autonomous self-healing elastomer. *Chem.* **8**, 618-624 (2016).
18. Rich S. I, *et al*. Untethered soft robotics. *Electron.* **1**, 102-112 (2018).
19. Christianson C, *et al*. Translucent soft robots driven by frameless fluid electrode dielectric elastomer actuators. *Robot.* **3**, eaat1893 (2018).
20. Gu G, *et al*. Soft wall-climbing robots. *Robot.* **3**, eaat2874 (2018).
21. Plante J-S, *et al.* On the performance mechanisms of dielectric elastomer actuators. *Actuat. A-Phys.* **137**, 96-109 (2007).
22. Bauer S, *et al*. Ferroelectrets: soft electroactive foams for transducers. *Today* **57**, 37-43 (2004).
23. Li W, *et al*. Nanogenerator-based dual-functional and self-powered thin patch loudspeaker or microphone for flexible electronics. *Commun.* **8**, 15310 (2017).
24. Cao Y, *et al*. Understanding the dynamic response in ferroelectret nanogenerators to enable self-powered tactile systems and human-controlled micro-robots. *Nano Energy* **63**, 103852 (2019).
25. Zhang X, *et al*. Vibration-based energy harvesting with piezoelectrets having high d_{31} *Appl. Phys. Lett.* **108**, 193903 (2016).
26. Zhong J, *et al.* Surface charge self-recovering electret film for wearable energy conversion in a harsh environment. *Energy Environ. Sci.* **9**, 3085-3091 (2016).
27. Gescheider G, et al. Information-processing channels in the tactile sensory system: A psychophysical and physiological analysis. Psychology Press, New York (2009).
28. Chortos A, *et al*. Pursuing prosthetic electronic skin. *Mater.* **15**, 937-950 (2016).
29. Verrillo RT. Investigation of some parameters of the cutaneous threshold for vibration. *Acoust. Soc. Am.* **34**, 1768-1773 (1962).
30. Makous JC, *et al.* The effects of static indentation on vibrotactile threshold. The *Acoust. Soc. Am.* **99**, 3149-3153 (1996).
31. Lin L, **et al**. Comparative study of hot embossed micro structures fabricated by laboratory and commercial environments. *Technol.* **4**, 113-116 (1998).
32. Li W, *et al*. Theoretical study of cellular piezoelectret generators. *Funct. Mater.* **26**, 1964-1974 (2016).

33. https://en.wikipedia.org/wiki/Extra-low_voltage, accessed in Dec. 2020.
34. Hollins S. Vibrotactile adaptation impairs discrimination of fine, but not coarse, textures. *Mot. Res.* **18**, 253-262 (2001).
35. Verrillo R., *et al.* Effect of prior stimulation on vibrotactile thresholds. *Sensory Processes* **1**, 292-300 (1977).
36. Gescheider G., *et al*. Selective adaptation of vibrotactile thresholds. *Sensory Processes* **3**, 37-48 (1979).
37. Leroy E*, et al.* Multimode hydraulically amplified electrostatic actuators for wearable haptics. *Mater.* **32**, 2002564 (2020).
38. Mun S, *et al.* Electro-active polymer based soft tactile interface for wearable devices. *IEEE T. Haptics* **11**, 15-21 (2018).
39. Pyo D, *et al.* High-pressure endurable flexible tactile actuator based on microstructured dielectric elastomer. A *Phys. Lett.* **112**, 061902 (2018).
40. Yun S, *et al.* A Soft and transparent visuo-haptic interface pursuing wearable devices. *IEEE T. Ind. Electron.* **67**, 717-724 (2020).
41. Matysek M, et al. Tactile display with dielectric multilayer elastomer actuators. SPIE (2009).
42. Yoon SH, *et al*. HapSense: A soft haptic I/O device with uninterrupted dual functionalities of force sensing and vibrotactile actuation. Proceedings of the 32nd Annual ACM Symposium on User Interface Software and Technology, (2019).
43. Ankit, Tiwari N, *et al.* Highly transparent and integrable surface texture change device for localized tactile feedback. *Small* **14**, 1702312 (2018).
44. Han AK, *et al*. Haptic surface display based on miniature dielectric fluid transducers. *IEEE Robot. Autom. Lett.* **5**, 4021-4027 (2020).
45. Guo X, *et al.* Absolute and discrimination thresholds of a flexible texture display. In: 2017 IEEE World Haptics Conference (WHC) (ed^(eds) (2017).
46. Park W, *et al*. Soft haptic actuator based on knitted PVC gel fabric. I*EEE T. Ind. Electron.* **67**, 677-685 (2020).
47. Ganet F, *et al*. Haptic feedback using an all-organic electroactive polymer composite. *Actuat. B-Chem.* **220**, 1120-1130 (2015).
48. Park W-H, *et al*. Development of a flexible and bendable vibrotactile actuator based on wave-shaped poly(vinyl chloride)/acetyl tributyl citrate gels for wearable electronic devices. *Smart Mater. Struct.* **25**, 115020 (2016).
49. Zhao H, *et al.* A Wearable Soft Haptic Communicator Based on Dielectric Elastomer Actuators. *Soft Robot.* **7**, 451-461 (2020).
50. Phung H, *et al*. Interactive haptic display based on soft actuator and soft sensor. In: 2017 IEEE/RSJ International Conference on Intelligent Robots and Systems (IROS) (ed^(eds) (2017).

51. Park W-H, *et al*. A Soft Vibrotactile Actuator with Knitted PVC Gel Fabric. In: Haptics: Science, Technology, and Applications (ed^(eds Prattichizzo D, Shinoda H, Tan HZ, Ruffaldi E, Frisoli A). Springer International Publishing (2018).
52. Rychkov D, *et al.* Chemical and physical surface modification of PTFE films—an approach to produce stable electrets. *Phys. A* **107**, 589-596 (2012).
53. Xia Z, *et al.* Charge storage and its dynamics in porous polytetrafluoroethylene (PTFE) film electrets. *IEEE T. Dielect. El. In.* **10**, 102-108 (2003).
54. Knez L, *et al*. Sequential Approach to the Biodynamic Modeling of a Human Finger. *Shock Vib.* **2017**, 8791406 (2017).
55. http://www.ti.com/lit/an/sloa194/sloa194.pdf, accessed in Dec. 2020.

Figures

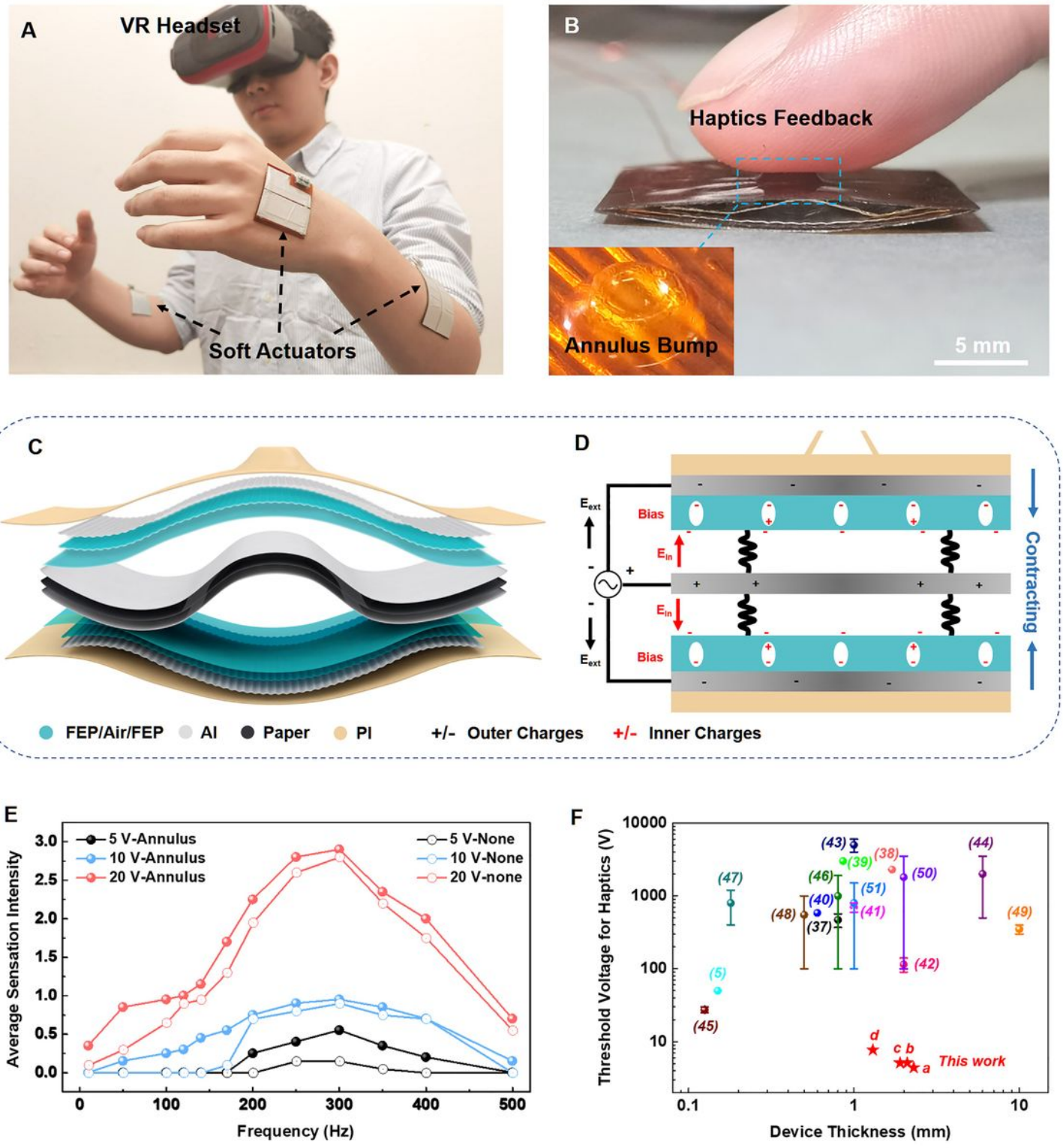

Figure 1

An electret-based soft actuator patch with a low driving voltage for haptics human-machine interfaces. (A) An optical photo illustrating the potential applications of the soft actuator patches attached on the human skin for human machine interfaces applications like virtual reality. (B) A prototype actuator is pressed by the fingertip of a volunteer for haptics feedback. Inset: the oblique view showing the annulus-shape bump structure. (C) The schematic diagram of the soft actuator: two FEP/Air/FEP/Al/PI films at

the top and bottom sandwiching a wavy-shape Al/paper/Al spring structure at the center. (D) The soft actuator under a preload by the fingertip, where Ein is the built-in electrical field generated by the electrostatic charges on the electret materials and Eext is the external electrical field generated by the applied driving voltage. Under an applied AC voltage, the soft actuator will generate vibrational motions due to the alternating electrostatic force. (E) The average sensation intensity from 20 volunteers under the driving voltages of 5, 10, 20 Volts and frequency of 10-500 Hz for the soft actuator patch with (solid symbols) and without (open symbols) the annulus-shape bump structure. (F) The smallest threshold voltages to generate haptic sensations on human skins from the state-of-art soft actuators. Red star symbols are results from the prototype soft actuators of this work with different bump designs including: (a) an annulus-shape bump with width/outer diameter of 0.5/4 mm and a total contact area of 5.5 mm2; (b) an annulus-shape bump with width/outer diameter of 0.5/8 mm and a total contact area of 12 mm2; (c) a cylinder-shape bump with a total contact area of 5.5 mm2; and (d) a flat surface without any bump structure.

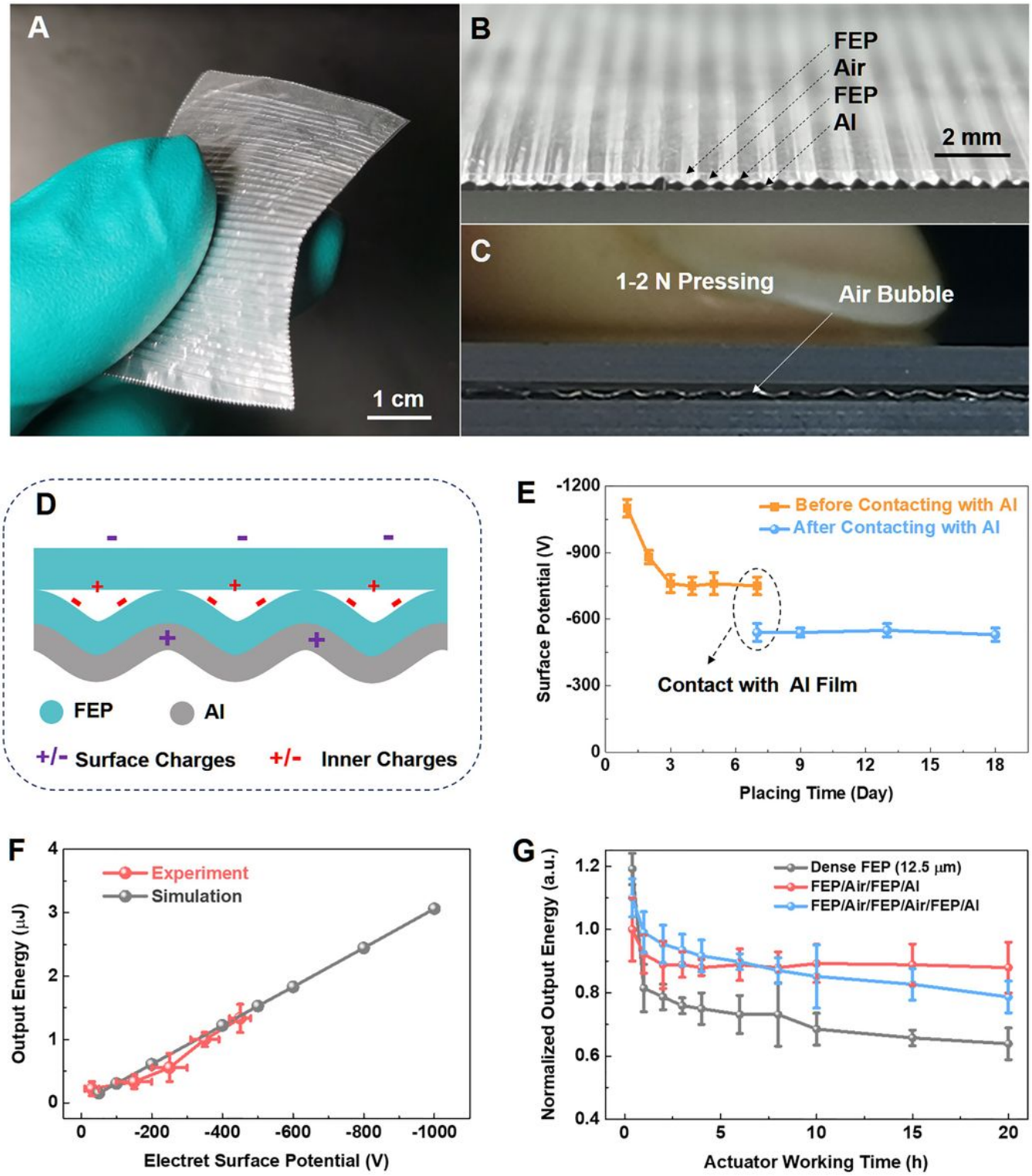

Figure 2

Effects of electret structure design. (A) Optical image of a prototype FEP/Air/FEP/Al electret film. (B) Enlarged image showing the film composed of a flat FEP film and a wavy-shape FEP/Al film. These two films are adhered together with air bubbles in between during the Corona charging process. (C) An optical image of the FEP/Air/FEP/Al film pressed by the fingertip of a volunteer to illustrate that both the wavy-shape structure and air bubbles are preserved. (D) Electrostatic charge distributions in the FEP/Air/FEP/Al

film showing many charges stored on the inner surface of the air bubbles. (E) Surface potential vs. time for the FEP/Air/FEP/Al film before and after physical contacts with an Al film. (F) Experiment and simulation results for the output energy of prototype actuators (size of 2×2 cm2) with respect to the electret surface potential. (G) Normalized output energy vs. time for soft actuators based on a 12.5 μm-thick and single-layer FEP film, a FEP/Air/FEP/Al film (one-layer air bubbles), and a FEP/Air/FEP/Air/FEP/Al film (two-layers air bubbles), respectively.

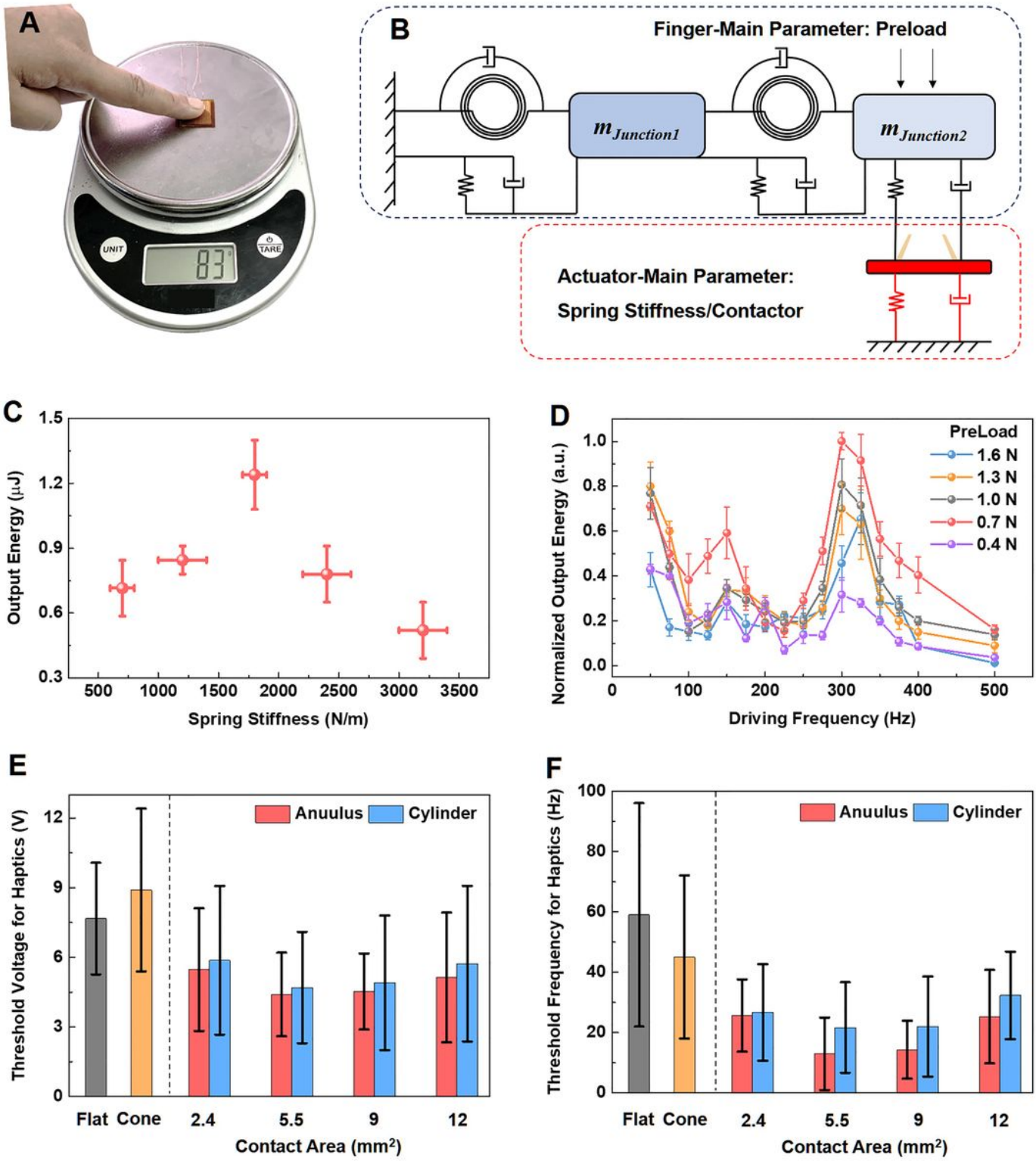

Figure 3

Effects of mechanical design and preload. (A) An optical image of the experimental setup to measure the preload value on a soft actuator. (B) A simplified model including the preload on the soft actuator of various mechanical parameters. (C) Measured output energy of the prototype soft actuators with respect to the spring stiffness under a preload of 0.7 N and a driving voltage of 20 Volts at 300 Hz. (D) Normalized output energy versus driving frequency under various preload values with a spring stiffness of 1800 N/m and a driving voltage of 50 Volts. (E) The threshold driving voltage at a driving frequency of 300 Hz, and (F) the lowest frequency to induce haptic sensations under a fixed driving voltage of 20 Volts based on 15 volunteers for soft actuators with flat surface, cone-shape, cylinder-shape and annulus-shape bump with the contact areas of 2.4, 5.5, 9, and 12 mm2, respectively.

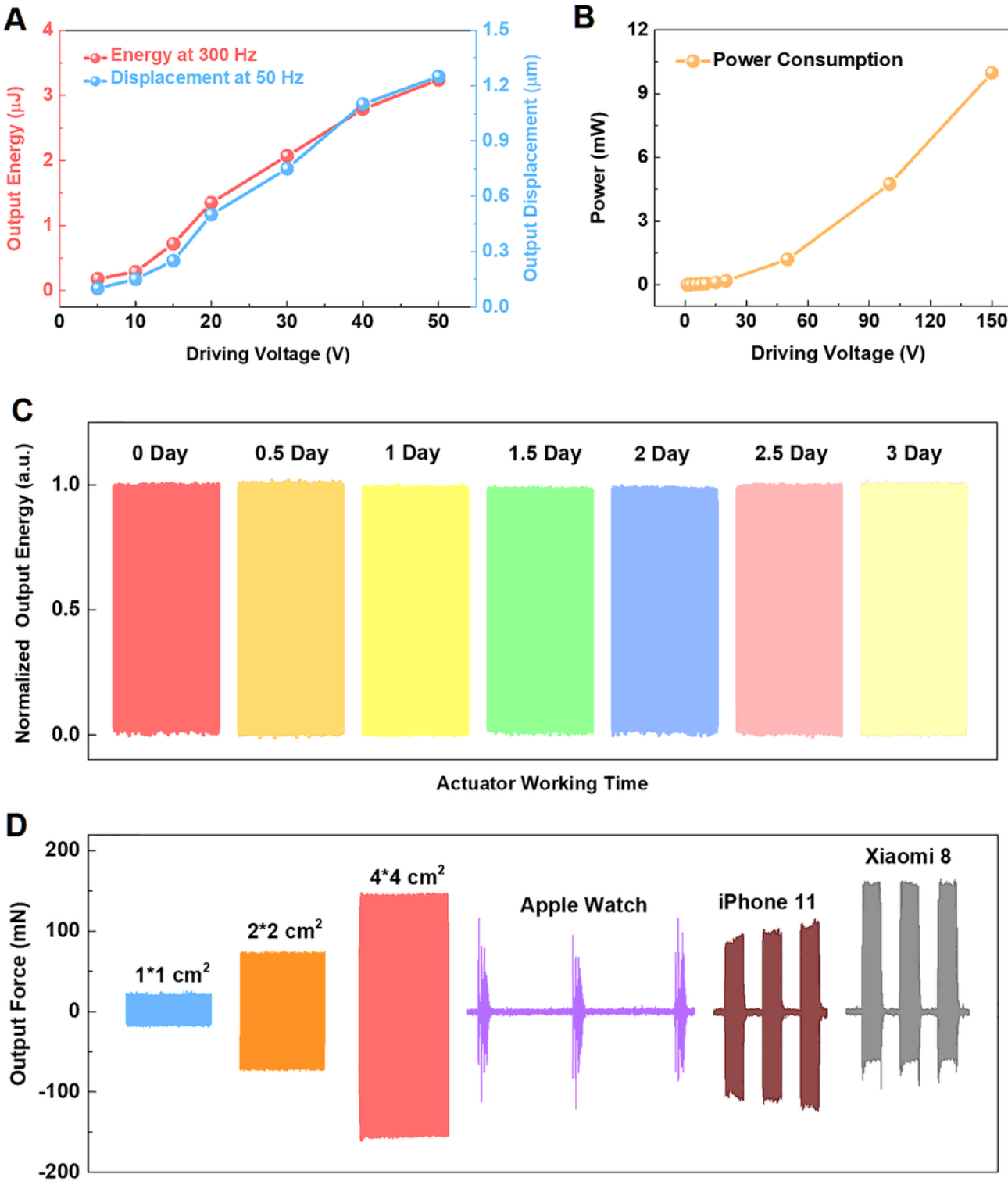

Figure 4

Excellent output abilities. (A) Measured output energy and displacement for a 2×2 cm2 prototype soft actuator (spring stiffness of 1800 N/m) versus applied voltage at frequencies of 300 Hz (sensitive for PC receptors) and 50 Hz (sensitive for MC receptors), respectively, with a preload of 0.7 N. (B) The power consumption of the prototype actuator versus applied voltage at 300 Hz and preload of 0.7 N. (C) Normalized output energy vs. time for a 2×2 cm2 prototype actuator during a continuous 3-days stability

test, under a constant voltage of 50 Volts at 300 Hz, and a preload of 0.7 N. (D) Measured output force for prototype actuators with various sizes under a driving voltage of 150 Volts compared with results from a smart watch, and two cellphones.

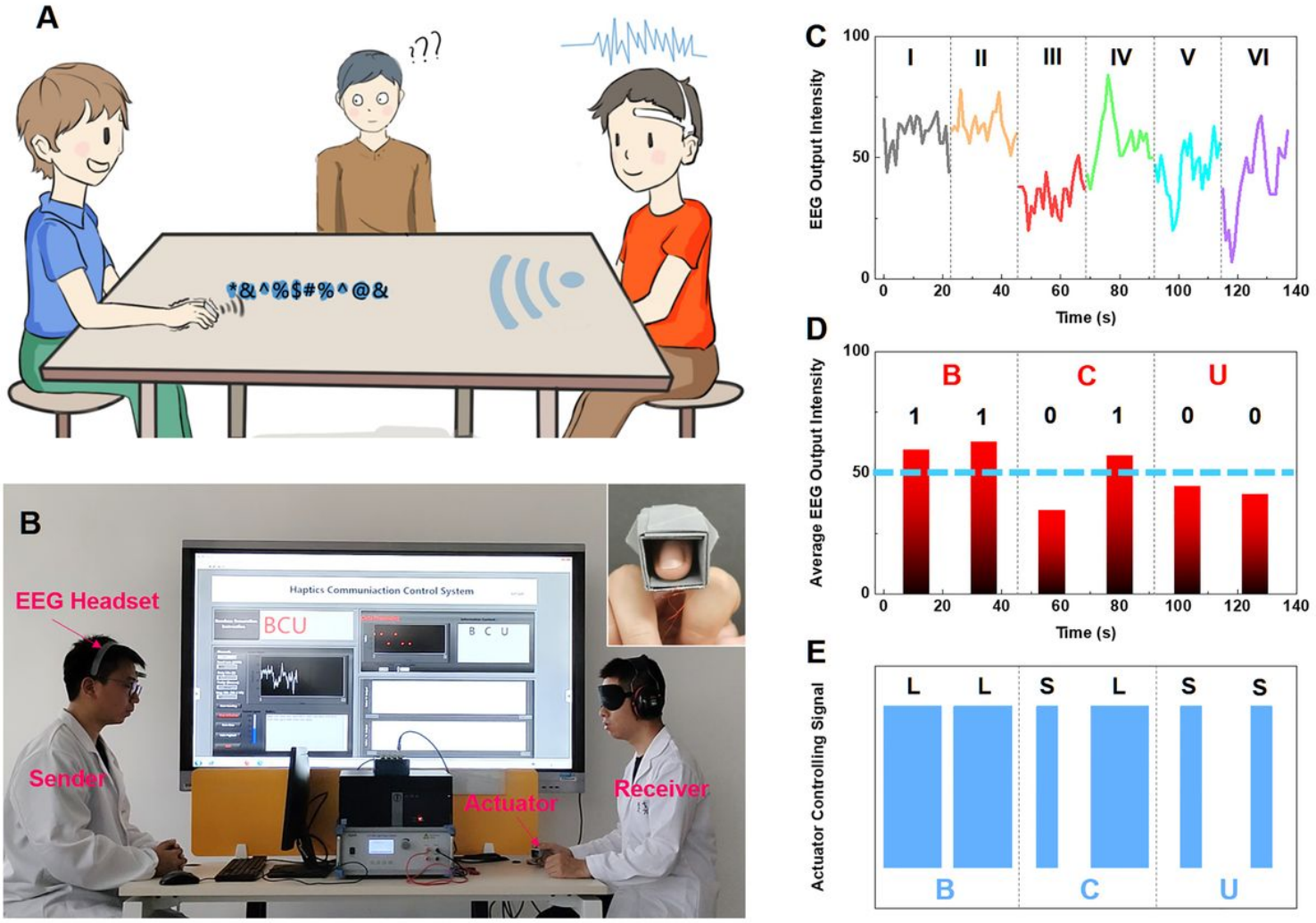

Figure 5

A wearable silent haptic communication system. (A) The schematic diagram depicting the concept of the wearable silent haptic communication system. (B) An optical photo showing the silent haptic communication system setup based on the soft actuator and an EEG headset. The EEG headset can record the concentration levels of a volunteer as the sender and the signals are converted to specific codes for the silent communication. The actuator placed on the finger of another volunteer as the receiver can generate haptic sensation patterns according to the EEG signals to transmit the information. (C) Recorded EEG output intensity from the sender and the average value of 20-second cycle is used to define either “1” or “0”. (D) The average EEG intensity values for 6 cycles to be characterized as “1” or “0” based on the value of 50. In this work, “B” is coded as “11”, “C” is coded as “01”, and “U” is coded as “00”, respectively. (E) Recorded examples for “1” and “0” by using 10-second (L) and 3-second (S) stimulation patterns as “1” and “0”, respectively.

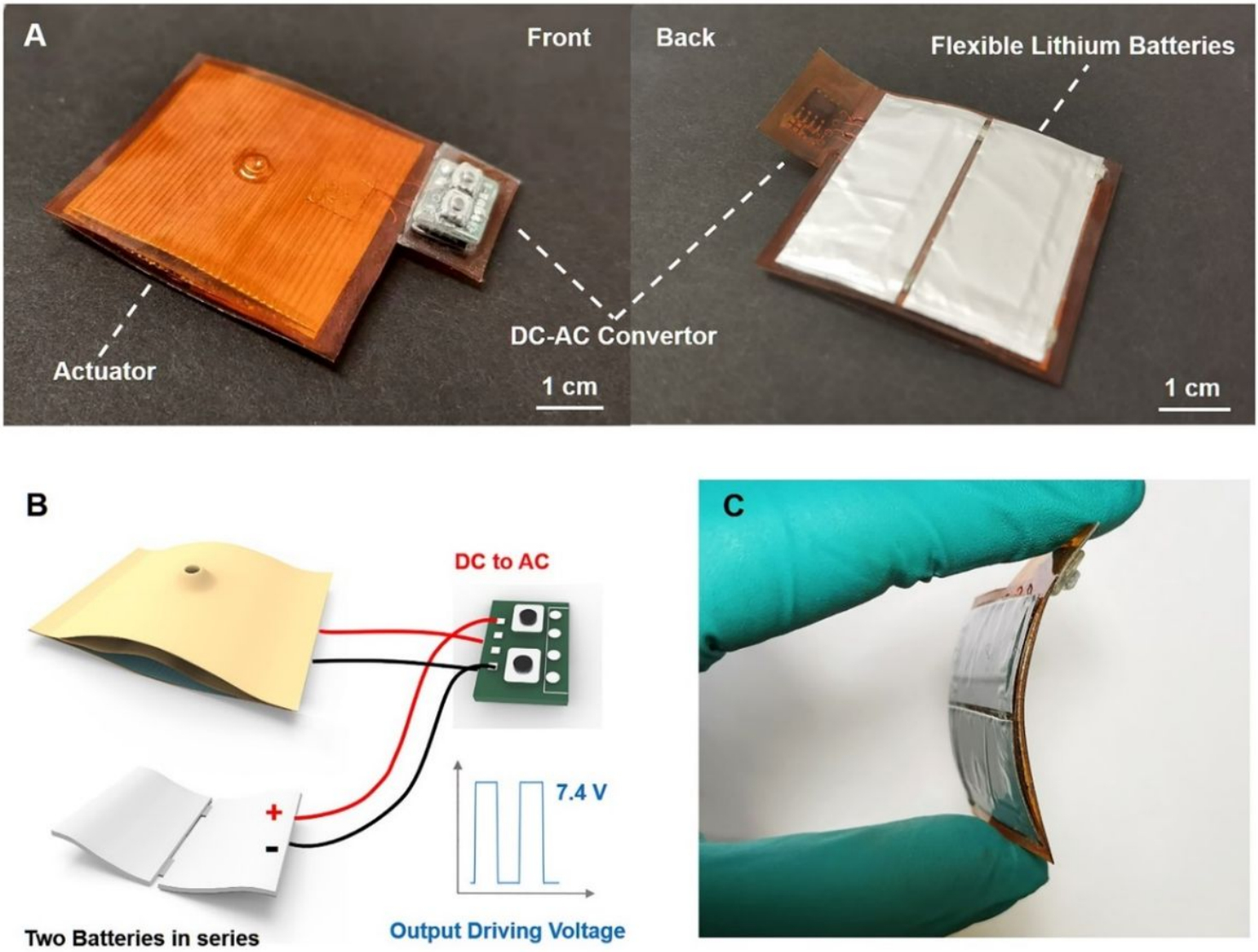

Figure 6

(A) Optical photos showing the front and back side of an untethered actuator patch. (B) The design of a portable untethered actuator patch by converting a DC voltage of 7.4 Volts to AC signals of different frequencies. (C) An optical photo showing the flexibility of the untethered actuator patch.

Supplementary Files

This is a list of supplementary files associated with this preprint. Click to download.

- SupportingVideo1.mp4
- SupportingVideo2.mp4
- SupportingVideo3.mp4
- SupplementaryMaterialsNE.docx